Interfacial sources of extended defects in nonpolar and semipolar III-Nitride semiconductors

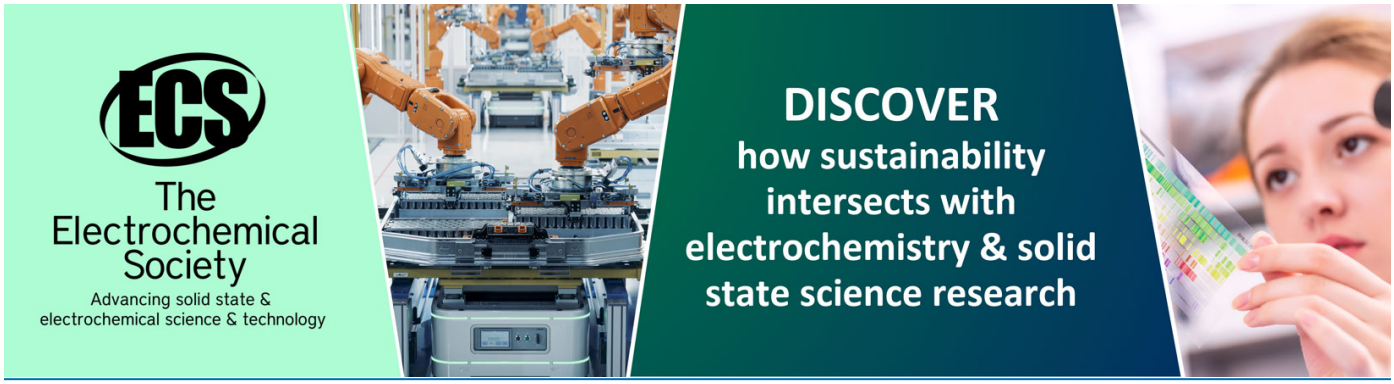

Journal of Physics: Conference Series **281** (2011) 012012 doi:10.1088/1742-6596/281/1/012012

Interfacial sources of extended defects in nonpolar and semipolar III-Nitride semiconductors

G P Dimitrakopulos

Physics Department, Aristotle University of Thessaloniki, GR 541 24, Thessaloniki, Greece

E-mail: gdim@auth.gr

Abstract. The principal characteristic of nonpolar and semipolar heteroepitaxial interfaces is their anisotropy that leads to distinct ways of misfit accommodation along two in-plane directions. One direction can require misfit dislocations with out-of-plane Burgers vectors that induce epilayer tilts and low-angle grain boundaries, and the other necessitates the introduction of multiple basal-plane stacking faults. The reduced bicrystalline symmetry also favours the coexistence of distinct epilayer orientation relationships. This may result in nanocrystalline interfacial zones comprising low-energy grain boundaries that act as defect sources for the matrix epilayer, generating threading dislocations and stacking faults.

1. Introduction

III-Nitride compound semiconductors with wurtzite structure are promising materials for extending the operational range of optoelectronic devices from UV to IR wavelengths. Towards this goal, a principal obstacle is the strain-induced piezoelectric polarization at quantum nanostructures (wells and dots) grown along the polar *c*-axis orientation. It leads to carrier separation and band structure distortion, reducing dramatically the internal quantum efficiency with increasing alloy content [1, 2]. Therefore III-Nitride heterostructures grown along nonpolar orientations are currently under intense investigation [2-4]. Semipolar orientations, whereby the *c*-axis is inclined relative to the heteroepitaxial interface, are another option, offering partial reduction of the polarization field. High quality heterostructure deposition on foreign substrates such as sapphire is required for effective technological advancement. To date such epilayers exhibit threading dislocation densities in excess of 10^{10} cm^{-2} and stacking fault densities of ~10^{5} cm^{-2} .

The principal characteristic of these heterostructures compared to polar III-N epitaxy is that they exhibit distinct ways of misfit accommodation along different in-plane directions. The strain anisotropy and the reduced bicrystal symmetry lead to novel relaxation mechanisms, and we review and generalize such mechanisms for nonpolar and semipolar epilayers, based on recent results obtained for *a*-plane GaN grown on sapphire [5, 6]. For this purpose we employ transmission electron microscopy (TEM) observations and topological analysis in order to elucidate the role played by III-N/sapphire interfaces in the introduction of defects in nonpolar and semipolar epilayers.

For the purpose of demonstrating general conclusions, representative heterostructures are considered, namely (i) nonpolar *a*-plane $(11\bar{2}0)$ GaN grown on *r*-plane $(1\bar{1}02)$ sapphire, and (ii) semipolar $(11\bar{2}2)$ AlN grown on *m*-plane $(1\bar{1}00)$ sapphire [5-7]. The heteroepitaxial orientation relationships are (i) $[0001]_{\text{III-N}}//[1\bar{1}0\bar{1}]_{\text{sapph.}}$, $[1\bar{1}00]_{\text{III-N}}//[\bar{1}\bar{1}20]_{\text{sapph.}}$ for *a*-plane epilayers, and (ii)

$[\bar{1}\,\bar{1}\,23]_{\text{III-N}}//[0001]_{\text{sapph.}}$, $[1\bar{1}00]_{\text{III-N}}//[\bar{1}\,\bar{1}\,20]_{\text{sapph.}}$ for $(11\bar{2}2)$ growth. The layers have been grown by plasma-assisted molecular beam epitaxy (PAMBE) as described elsewhere [5-7].

2. Emanation of stacking faults

In both the nonpolar and semipolar orientations, two misfit dislocation arrays, with edge Burgers vector components vertical to one another, suffice for misfit accommodation. However, the two vertical in-plane directions exhibit distinct structures. Moreover, the misfit differs significantly along each direction. In *a*-plane GaN grown on *r*-plane sapphire, the misfit along $[0001]_{\text{GaN}}$ is only +1.2% and reaches +16% along $[1\bar{1}00]_{\text{GaN}}$. In $(11\bar{2}2)$ AlN grown on *m*-plane sapphire, the mismatch is tensile +13.4% along $[1\bar{1}00]_{\text{AlN}}$ and compressive -9.6% along $[\bar{1}\,\bar{1}\,23]_{\text{AlN}}$.

Accommodation of the misfit along the [0001] *c*-axis in the case of nonpolar heteroepitaxy, or along the in-plane projection of the *c*-axis in the case of semipolar, necessitates the introduction of misfit dislocations with edge Burgers vector components that comprise single (0002) extra half-planes. However, since the lattice dislocations with [0001] Burgers vector components require two extra half-planes (due to the …*ABAB*… hexagonal stacking), such misfit dislocations can only be partials with Burgers vectors of type **b** = $1/6<2\bar{2}03>$. Each such partial must be associated with a stacking fault. There is then the possibility that the stacking fault is superimposed on the heteroepitaxial interface, or it emanates into the epilayer, as shown schematically in Figures 1(a) and (b) respectively. In the latter case, the basal stacking faults are of I_1 (0002) intrinsic type, since they are delimited by Frank partials [8]. Although the latter process necessitates dislocation climb, the TEM measurements show that the stacking fault density is consistent with this being a principal process of misfit relaxation [5]. The stacking fault emanation from the heteroepitaxial interface was verified by plan-view high resolution TEM (HRTEM) observations of *a*-plane GaN epilayers showing termination of Moiré fringes at the delimiting partial dislocations of edge-on I_1 stacking faults [5].

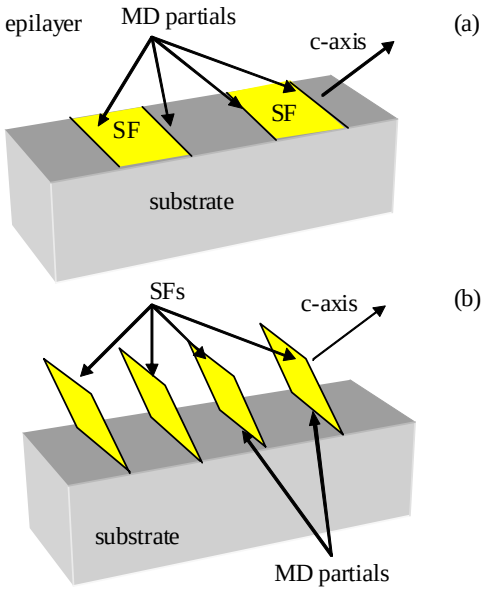

Figure 1. Schematic of the plausible mechanisms of misfit accommodation along the *c*-axis (nonpolar epilayer) or its in-plane projection (semipolar epilayer). The misfit dislocations (MDs) are $1/6<2\bar{2}03>$ partials. In (a) the associated stacking faults (SFs) are parallel to the heteroepitaxial interface thereby introducing alternating interfacial structure. In (b) the SFs are parallel to the (0002) basal plane and emanate into the epilayer.

3. Misfit dislocations with inclined Burgers vectors

A second relaxation mechanism concerns the misfit along the in-plane direction vertical to the *c*-axis. In this case the misfit dislocations have line directions along [0001] or its in-plane projection. The shortest lattice Burgers vectors are the **b** = $1/3<\bar{1}2\bar{1}0>$ vectors. However, in both the $(11\bar{2}0)$ and $(11\bar{2}2)$ epitaxies, such Burgers vectors do not lie in the heteroepitaxial interface. In fact the

$1/3<\bar{1}2\bar{1}0>$ Burgers vectors are in-plane only for prismatic *m*-plane $\{1\bar{1}00\}$ and for pyramidal type $\{1\bar{1}0w\}$ growth orientations. In all other nonpolar or semipolar epitaxial orientations the $1/3<\bar{1}2\bar{1}0>$ vectors are inclined relative to the substrate, and an example is shown in Figure 2 which illustrates a misfit dislocation array at the $(11\bar{2}2)$AlN/*m*-sapphire interface. A Burgers circuit has been drawn around one misfit dislocation showing the inclined Burgers vector. Such misfit dislocations comprise two edge components. The first component is in-plane accommodating the misfit, while the second is normal to the interface. In the case of Figure 2, these components have magnitudes 0.269 nm and 0.132 nm respectively.

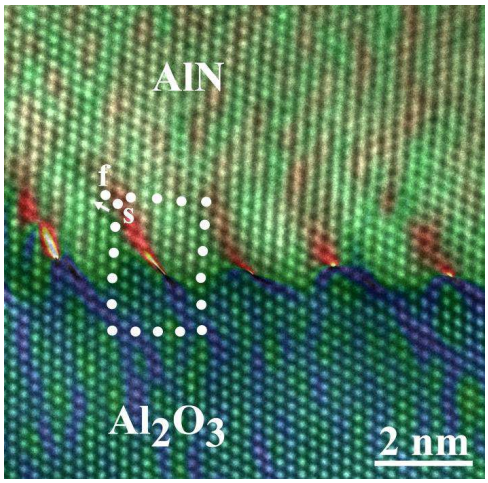

Figure 2. Cross sectional HRTEM image of $(11\bar{2}2)$AlN / *m*-plane sapphire viewed along $[\bar{1}\bar{1}23]_{AlN}/[0001]_{sapph.}$. The image shows a periodic array of misfit dislocations. The two-dimensional map of the lattice strain along the $[1\bar{1}00]_{AlN}$ in-plane direction is superimposed (this map has been obtained by geometrical phase analysis [9]). Circuit mapping identifies the Burgers vector of the misfit dislocations as an inclined vector **sf** of $1/3<\bar{1}2\bar{1}0>$ type.

As a result of the normal Burgers vector component, such misfit dislocation arrays induce lattice tilts by acting effectively as low-angle tilt boundaries [5]. Since the sapphire substrate is practically unaffected due to its large thickness and rigidity, the rotational effect of the misfit dislocation array is adopted by the epilayer. Figure 3 illustrates schematically the Volterra operations that introduce a misfit dislocation with inclined Burgers vector in *a*-plane GaN, in accordance with the topological theory of interfacial defects [10]. In this case the induced epilayer tilt is in opposite sense relative to the Burgers vector, since the extra half-plane is in the substrate. For a regular array of misfit dislocations with parallel Burgers vectors and spacing *d*, the maximum induced epilayer tilt is $\vartheta_{max} = b_n / d$ where b_n is the magnitude of the normal to the interface component of the Burgers vector. This tilt may be clockwise or anticlockwise depending on the upward or downward sense of the Burgers vector. However, if upward and downward-oriented Burgers vectors co-exist in the misfit dislocation array, then the rotational effect locally cancels out. Hence a range of misorientations of angles $\vartheta \leq \vartheta_{max}$ is anticipated. For *a*-plane GaN on *r*-plane sapphire, the misfit dislocations accommodating the 16% misfit introduce tilts by up to $\pm 5.4^o$ as verified by selected-area electron diffraction patterns obtained from epilayers grown by PAMBE under N-rich conditions [5]. For semipolar AlN the misfit is 13.4% corresponding to an average misfit dislocation spacing of 2 nm; hence $\vartheta_{max} = 3.8^o$.

Since the tilt induced by misfit dislocations may be clockwise or anticlockwise, low-angle tilt grain boundaries (LAGBs) of tilt angle $\leq 2\vartheta_{max}$ are introduced between abutting islands as shown schematically in Figure 4. Such LAGBs consist of lattice dislocations with their line directions parallel to the heteroepitaxial interface and their occurrence has been confirmed by HRTEM in *a*-plane GaN [5]. The LAGB dislocations may later participate in dislocation interactions and bend upwards to become threading dislocations.

In the case of semipolar epitaxies, the $1/3<\bar{1}2\bar{1}0>$-type misfit dislocations also comprise screw components since the basal planes on which these Burgers vectors lie are inclined relative to the substrate. The magnitude of the screw component increases with increasing inclination angle of the basal plane. Hence such arrays are capable of introducing twists in the orientation of the epilayer

crystal planes. For example, in the representative case of $(11\bar{2}2)$ AlN on sapphire, the magnitude of this screw component is b_s = 0.082 nm, and the maximum twist angle normal to the $[\bar{1}\,\bar{1}23]$ dislocation lines is $\phi_{max} = b_s / d = 2.35^o$. This twist may be compensated by extra defects.

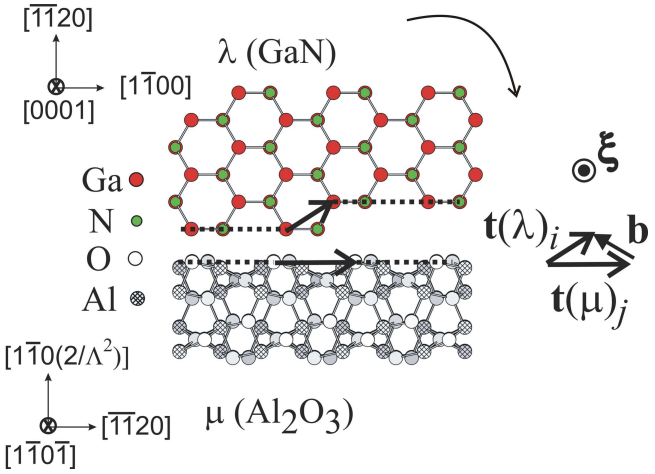

Figure 3. Volterra-like schematic illustration showing the translation operations $\mathbf{t}(\lambda)_i$ and $\mathbf{t}(\mu)_j$ that introduce a $\mathbf{b} = 1/3\langle\bar{1}2\bar{1}0\rangle$ misfit dislocation in *a*-plane GaN grown on *r*-plane sapphire. The curved arrow shows the sense of epilayer tilt. [Circle size and colouring denote distinct atomic species as indicated on the image, shading denotes distinct levels along the projection direction, vector ξ denotes the out-of-paper sense of the dislocation's line direction, and $\Lambda = (2/3)^{1/2}\,(c/a)_{sapph.}$].

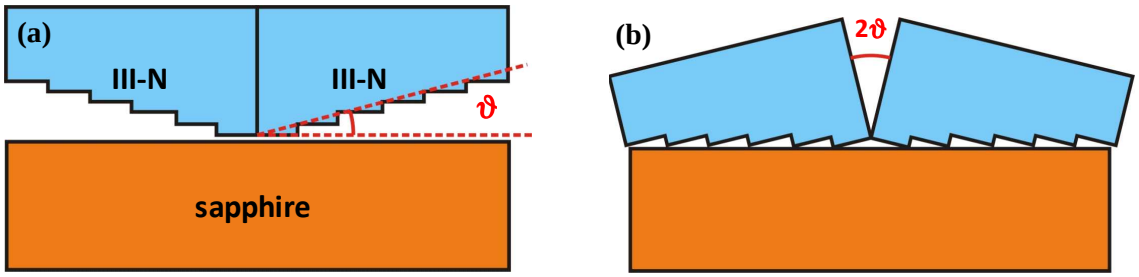

Figure 4. (a) Volterra-like schematic showing the clockwise and anticlockwise rotational senses induced by two misfit dislocation arrays with opposite Burgers vector senses in two abutting III-N islands. (b) Sequential accommodation of the two Volterra cuts and introduction of a relative tilt 2ϑ between the two islands. This 2ϑ wedge is filled by dislocated material comprising a LAGB.

4. Intergranular boundaries as defect sources

Anisotropy also favours the coexistence of distinct epilayer orientation relationships. In fact, just one low misfit in-plane direction can suffice for the introduction of a second epitaxial orientation. Depending on the growth conditions, one orientation may eventually dominate, but TEM observations in MBE-grown epilayers [5-7] have shown that the secondary orientation can still persist close to the substrate in the form of interfacial nanocrystals that are quickly overgrown. Such nanocrystals are surrounded by intergranular boundaries that are defect sources for the matrix epilayer, causing introduction of threading dislocations, stacking faults, nanotwins, and cubic pockets [5].

Figure 5(a) illustrates an HRTEM image of such a nanocrystal with an emanating threading dislocation inside PAMBE-grown *a*-plane GaN epilayer. The nanocrystal has a semipolar orientation described by a $90^o\ \langle 2\bar{1}\,\bar{1}0\rangle$ rotation relative to the $(11\bar{2}0)$ epilayer. Interestingly, the same orientation relationship was also observed between semipolar $(11\bar{2}2)$ and nonpolar *m*-plane $(1\bar{1}00)$ AlN nanocrystals grown on *m*-sapphire [7]. The $90^o\ \langle 2\bar{1}\,\bar{1}0\rangle$ relationship ensures a high order of coincident symmetry between the matrix epilayer and the nanocrystals, as illustrated in Figure 5(a). As a result, the (0002) planes in each crystal component are matched to the $\{10\bar{1}0\}$ planes in the other crystal with a 6.5% misfit for GaN and 8.2% for AlN. This misfit introduces dislocations at the

intergranular boundaries as illustrated by geometrical phase analysis in Figure 5(b). Furthermore, the intergranular boundaries appear to promote the introduction of stacking faults. In fact the overlap of multiple stacking faults can lead to …*ABCABC*… cubic stacking resulting to 'pockets' of sphalerite structure as illustrated in Figures 5(a) and 5(c).

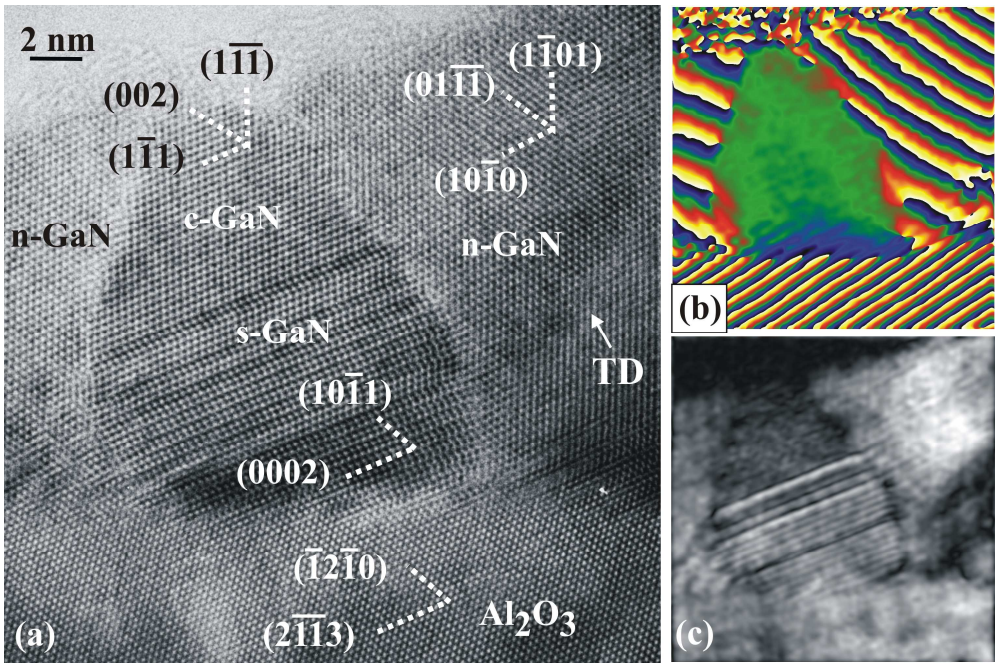

Figure 5. (a) HRTEM image of a semipolar interfacial nanocrystal (s-GaN) viewed along $[\bar{1}2\bar{1}0]$. Nonpolar $(11\bar{2}0)$ GaN (n-GaN) is viewed along $[\bar{1}2\bar{1}3]$ whereas $(1\bar{1}02)$ sapphire is viewed along $[10\bar{1}\bar{1}]$. The sphalerite-cubic part of the nanocrystal (c-GaN) is viewed along [110]. A threading dislocation (TD) emanates from the semipolar/nonpolar intergranular boundary (arrowed). (b) Phase map of (a) obtained using the $0002/10\bar{1}0$ GaN spatial frequencies. Fringe terminations at the interfaces indicate the locations of interfacial dislocation cores. [(a) and (b) are reprinted with permission from Smalc-Koziorowska *et al.*, J. Appl. Phys. **107**, 073525, 2010. Copyright 2010, American Institute of Physics]. (c) Amplitude image where the distinct structures inside the nanocrystal (wurtzite in lower part and sphalerite in upper part) can be discriminated.

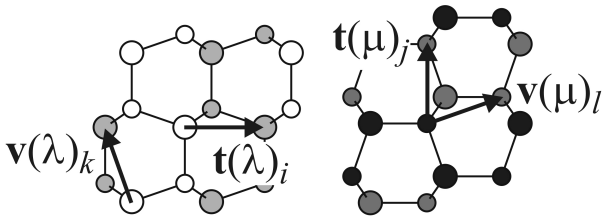

Figure 6. Schematic illustration showing the relative orientations of $\mathbf{t} = 1/3\langle\bar{1}2\bar{1}0\rangle$ lattice vectors and $\mathbf{v} = 1/6\langle2\bar{2}03\rangle$ structural vectors in two wurtzite crystals that are rotated by 90° about $\langle2\bar{1}\bar{1}0\rangle$.

An understanding of the influence of the intergranular boundaries on the introduction of threading dislocations and stacking faults can be attained by reference to the schematic illustration of Figure 6, whereby one crystal is arbitrarily designated as white (λ) and the other as black (μ). It is seen that, as a result of the 90° rotation, $1/3\langle\bar{1}2\bar{1}0\rangle$ lattice vectors in one crystal component are juxtaposed with $1/6\langle2\bar{2}03\rangle$ structural vectors in the other crystal and vice versa. Hence either vectors types may comprise the Burgers vectors of the interfacial dislocations that relieve the $(0002)/\{10\bar{1}0\}$ misfit. The

former vectors are the vectors of threading dislocations while the latter are responsible for the introduction of I_1 stacking faults as discussed earlier. Therefore, the intergranular boundaries can act as sources of such defects, without needing to satisfy complex nodal balance requirements. One possible mechanism for defect emanation is the wing coalescence due to lateral overgrowth of the nanocrystals by the matrix.

5. Conclusions

Based on the present review of nanoscale mechanisms we can deduce general conclusions and recommendations concerning the heteroepitaxial growth of nonpolar and semipolar III-Nitride epilayers. Regarding the large stacking fault density, this is an intrinsic property due to the misfit accommodation by partial dislocations comprising single (0002) extra half planes, and novel approaches involving interlayers and strain engineering are needed in order to overcome this problem. At the same time, the misfit dislocation arrays accommodating the mismatch along the in-plane direction vertical to the *c*-axis can induce tilting and twisting of epilayer planes due to their inclined Burgers vectors, and thus introduce extra extended defects, such as dislocations forming low-angle grain boundaries. In this regard the $\{1\bar{1}00\}$ and $\{1\bar{1}0w\}$ orientations are more promising heteroepitaxies. The third important issue concerns the control of the crystalline quality of the interfacial region with the substrate. Secondary epitaxial orientations appear easily due to the low common symmetry with the foreign substrate. Such an interfacial zone can even be difficult to detect since it may be confined to below 10 nm of epilayer thickness. However, the low energy of the intergranular boundaries, promoted by the $90^o < \bar{1}2\bar{1}0 >$ relative rotation, and their associated intrinsic dislocations make them potent defect sources for the epilayer. It is recommended that growth conditions, such as substrate pre-treatment, temperature, and flux ratios, are correlated to detailed HRTEM observations of the interfacial region with the substrate in order to optimize them towards eliminating any parasitic nanocrystals.

Acknowledgements

The author is grateful to J. Smalc-Koziorowska, Th. Kehagias, Ph. Komninou, and Th. Karakostas for invaluable input and critical reading, as well as to A. Georgakilas and E. Monroy for providing nonpolar and semipolar specimens grown by PAMBE. This work was performed under the support of EU projects DOTSENSE (Grant No. STREP 224212) and PARSEM (MRTN-CT-2004-005583).

References

[1] Humphreys C J 2008 *MRS Bulletin* **33** 459
[2] Speck J S and Chichibu S F 2009 *MRS Bulletin* **34** 304
[3] Masui H, Nakamura S, DenBaars S P, and Mishra U K 2010 *IEEE Trans. Electron. Devices* **57** 88
[4] Paskova T (ed) 2008 *Nitrides with Nonpolar Surfaces: Growth, Properties, and Devices* (Weinheim: Wiley)
[5] Smalc-Koziorowska J, Tsiakatouras G, Lotsari A, Georgakilas A, and Dimitrakopulos G P 2010 *J. Appl. Phys.* **107** 073525
[6] Smalc-Koziorowska J, Dimitrakopulos G P, Sahonta S-L, Tsiakatouras G, Georgakilas A, and Komninou Ph 2008 *Appl. Phys. Lett.* **89** 021910
[7] Kehagias Th, Lahourcade L, Lotsari A, Monroy E, Dimitrakopulos G P, and Komninou Ph 2010 *Phys. Stat. Sol.* **247** 1637
[8] Hirth J P and Lothe J 1982 *Theory of Dislocations*, 2nd Edition (New York: Wiley Intersciences) p 354
[9] Hÿtch M J, Putaux J-L, and Pénisson J-M 2003 Nature **423** 270
[10] Dimitrakopulos G P, Komninou Ph, Karakostas Th, and Pond R C 2003 Topological Analysis of Defects in Nitride Semiconductors *Nitride Semiconductors: Handbook on Materials and Devices*, ed P Ruterana, M Albrecht, and J Neugebauer (Weinheim: Wiley)